Iraqi Journal of Physics, 2026
https://doi.org/10.30723/ijp.v24i3.1376

Vol.24, No.3, PP.169-181
P-ISSN: 2070-4003
E-ISSN: 2664-5548

The Synergistic Effect of Nanoparticles (Ag:Se) Prepared by Plasma Jet Combined with *Plantago Lanceolata* on Parasitic *Leishmania Donovani*

Zahraa B. Jabeer[1*] and Naksheen M. Ardalan[1]
[1]*Department of Biology, College of Science for Women, University of Baghdad, Baghdad, Iraq*
[*]Corresponding author: Zahraa.jaber2202m@csw.uobaghdad.edu.iq

Abstract

Visceral leishmaniasis (VL) is a chronic infection caused by protozoa. Drug-resistant cases require an urgent solution to drug resistance and a therapeutic improvement strategy. Nanoparticles (NPs) containing synthetic plant extract exhibit antileishmanial potential as therapeutic agents. This study aims to investigate the synergistic antileishmanial effect of silver: selenium (Ag: Se) core-shell NPs synthesized using the plasma jet technique in combination with *Plantago lanceolata* leaf extract against *Leishmania donovani*. The Ag:Se NPs were synthesised and applied at two concentrations, 125 and 250 µg/mL, to assess their potential activity in vitro. The control treatment was miltefosine, an anti-leishmaniasis medication. *P. lanceolata* extract at concentrations of 125 and 250 µg/mL was used to produce Ag NPs as a core and add selenium as a shell. The generated Ag:Se NPs were characterised using UV-Vis spectroscopy, X-ray diffraction (XRD), transmission electron microscopy (TEM), and scanning electron microscopy (SEM). The anti-leishmanial activity of Ag:Se NPs was evaluated. Ag:Se NPs were assessed at 125 and 250 µg/mL concentrations, with 25%, 50%, and 100% serial dilutions over 1, 24, and 48 h incubation periods. After 48 hours, the percentage of inhibition for Ag:Se NPs (125 and 250 µg/mL) combined with the extract was 48.6% and 59.6%, respectively. Thus, it may be inferred from these results that the growth inhibition rate increases with the length of incubation of the parasite. Antileishmanial activity was improved in the case of Ag:Se NPs medicines designed using a plasma jet.

Article Info.

Keywords:
Ag:Se NPs, L. donovani, Plasma Jet, Synergism, TEM.

Article history:
Received: Dec. 15, 2024
Revised: Jul. 21, 2025
Accepted: Sep. 05, 2025
Published:Sep. 01,2026

1. Introduction

Leishmaniasis is a parasitic disease caused by protozoan parasites of the genus *Leishmania*, which are transmitted through the bite of infected female phlebotomine sand flies. There are three main clinical forms of leishmaniasis: cutaneous, mucocutaneous, and visceral. Visceral Leishmaniasis (VL), also known as kala-azar, is the most severe form of the disease, primarily caused by *Leishmania donovani* [1]. The World Health Organisation (WHO) has emphasized the urgent need for new drug candidates and innovative delivery systems to control and reduce the burden of leishmaniasis. The disease remains categorized as a Neglected Tropical Disease (NTD) due to its limited resources and attention, despite having a significant health impact in endemic regions [2]. However, it has been observed that the majority of leishmaniasis strains are resistant to standard chemotherapeutics, like paromomycin and antimonials, which has made treatment extremely difficult.

Nanotechnology, defined as the science and engineering of materials at the nanoscale (typically 1-100 nm), has significantly transformed drug discovery and therapeutic strategies over the past three decades [3, 4]. Newly developed nanoparticles (NPs) have shown promising potential in enhancing the delivery of medicinal compounds. By functionalizing nanoparticles with targeting ligands, drug delivery systems can achieve more precise targeting, improving efficacy and reducing side effects [5, 6]. Plasma jet is one of the cold plasma techniques widely used for nanoparticle synthesis due to its low temperature, high reactivity, and ability to process heat-sensitive materials. It generates a plasma plume by applying a high voltage across a gas (commonly argon, helium, or air), which allows the ionization of the gas and the formation of reactive species. These species facilitate the reduction and assembly of nanoparticles in a

controlled manner, making the plasma jet an environmentally friendly and efficient method for nanomaterial fabrication [7].

Plant extracts are becoming an increasingly popular choice for the creation of nanoparticles. Green synthesis, an eco-friendly and sustainable method, utilizes biological entities, such as plant extracts, bacteria, fungi, and algae, to synthesize nanoparticles without the need for toxic chemicals or high-energy inputs. Moreover, it has been proven that the use of plant extracts can influence the size, shape, and morphological properties of nanoparticles, thereby enabling better control over their characteristics [8]. One plant that has active chemicals is *Plantago lanceolata*. Leaf extract of *P. lanceolata* is rich in secondary metabolites, like sterols, polysaccharides, vitamins, phenolic compounds, lignin, flavonoids, and proteins, due to the quantity of active secondary metabolites it contains. These constituents serve as organic reductants and stabilizers and are crucial to the environmentally friendly synthesis of nanoparticles [9].

Silver Nanoparticles (AgNPs) synthesized via green synthesis using plant extracts hold great promise for heavy metal detection, targeted drug delivery, and antibacterial properties [10, 11]. Thus, biosynthesis—that is, the environmentally benign and non-toxic green synthesis of Ag NPs—has attracted a great deal of attention and study. Selenium Nanoparticles (SeNPs) have the potential to be a drug delivery vehicle for antioxidant or anti-inflammatory effects [12, 13]. Due to their ability to balance redox, SeNPs have been linked to a plethora of medical benefits, including anticancer and antioxidant activities [14]. Since SeNPs are larger on the surface and smaller on the inside, they interact with biological molecules by disrupting biofilms, rupturing cell walls, and compromising membranes, all of which stop the growth of pathogens [15].

In this study, the Ag:Se NPs and plant extract were utilized for two purposes: first, as a plant extract reducing and stabilizing agent in the green synthesis of Ag nanoparticles, and second, to evaluate the inhibitory effect of Ag-Se nanoparticles at two different concentrations against Leishmania. The plant extract was separately tested for its potential use as an antileishmanial agent.

2. Experimental Work

2.1. Extraction of *Plantago lanceolata* leaves

To prepare the *P. lanceolata* plant extract, the plant leaves were collected from the gardens of the University of Baghdad in February. The leaves were first cleaned and rinsed with distilled water. They were then thinly sliced and left to dry for a week. After the drying process was complete, the dry extract was collected and used for the research. A 20% (W/V) water extract was prepared from the dried leaves. The water extract was stored at 4 to 8°C until needed. Two concentrations of the extract solution were prepared: 125 and 250 µg/mL. Chemical detection of the active compounds of the *P. lanceolata* extract revealed phenolic compounds, flavonoids, polyphenols, terpenoids, tannins, carbohydrates, and saponins, some of which may cause colour changes or precipitate formation [16].

2.2. Preparation of Ag:Se core-shell NPs

Ag:Se core-shell NPs were synthesized in two stages. The first involved producing AgNPs using *P. lanceolata* leaf extract at concentrations of 125 and 250 µg/mL as the core. Using a plasma jet technique, they were exposed to plasma for 3 minutes. The plasma jet system operated at 10–20 kV and 25 kHz, using argon as the working gas at a flow rate of 3 L/min. Small stainless-steel tubes (10 cm x 1 mm) were used as electrodes to hold the beaker and provide electricity in a steady or pulsed flow. The second stage involved forming the shell by adding 5 mL of selenium nitrate to 5 mL of Ag NPs, followed by exposing the mixture to the plasma jet for 14 minutes. Fig. 1 illustrates this process. The reaction caused the color of the

solution to change to a yellowish-green. Characterization of Ag:Se core-shell NPs was performed using a UV-visible spectrometer (UV-1800, Shimadzu, United States) between 300 and 800 nm. Crystallinity and phase purity were assessed using X-ray diffraction (XRD) analysis with a 2700ab diffractometer. Further structural characterization, elemental mapping, and morphological analysis were conducted using a field emission scanning electron microscope (FE-SEM) (Zeiss Sigma 300-HV, Germany). Elemental mapping, morphological analysis, and transmission electron microscopy (TEM) were used for additional structural characterization.

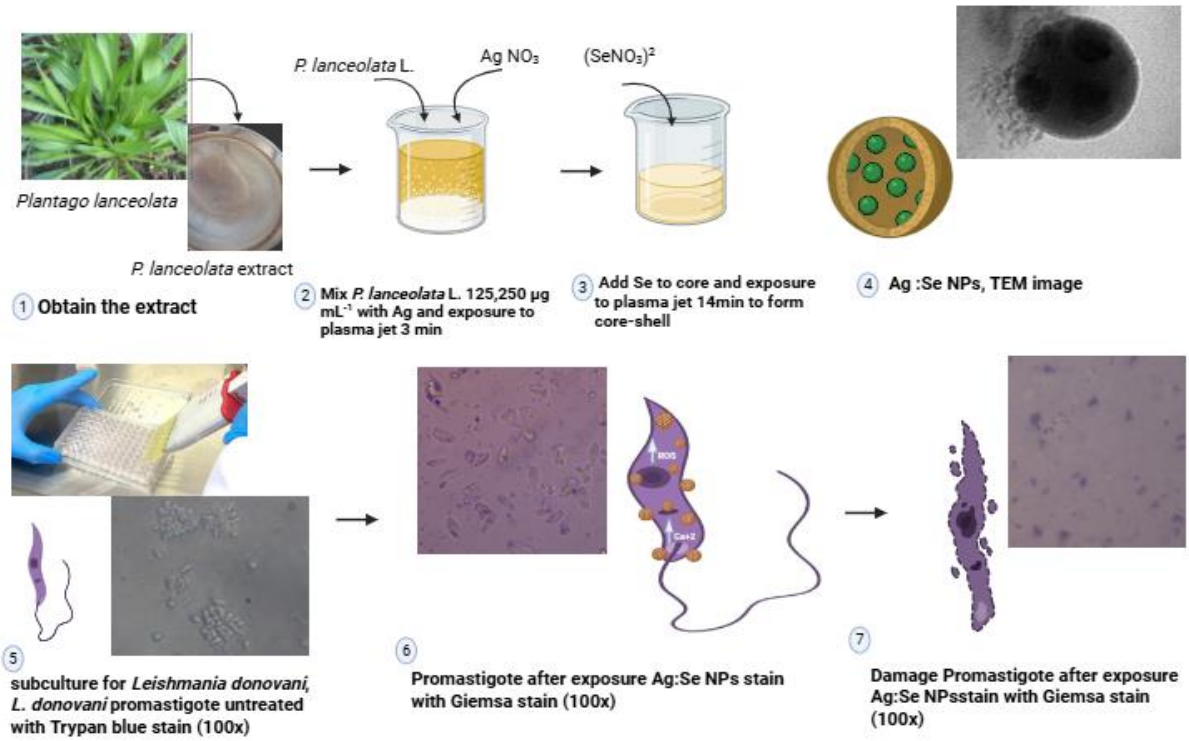

Figure 1: Schematic diagram of the preparation of Ag: Se NPs and their evaluation against the anti-leishmanial parasite (Created with BioRender).

2.3. Assessing the Impact of Nanomaterials on Leishmaniasis Parasite Inhibition

The standard strain of *L. donovani* promastigotes was cultured in vitro at the Biotechnology Research Centre of Al-Nahrain University. The promastigotes were transferred to RPMI-1640 culture medium, and the culture flasks were incubated at 25 ± 1°C. Daily observations were performed using an inverted microscope. Following cell distribution, the cells were seeded in a 96-well microtiter plate with 10,000 cells/well [17]. Four treatment groups were arranged: in the first group, Ag:Se NPs at concentrations of 125 and 250 µg/mL at dilutions of 25, 50, and 100% were applied to the cells. The second group, Ag:Se NPs was administered in combination with *P. lanceolata* extract at 125 and 250 µg/mL. The third group was exposed to *P. lanceolata* extract alone at the same concentrations. The fourth group was exposed to the standard drug miltefosine, the standard antileishmanial drug.

2.4. Cytotoxicity Evaluation of Treatments Against *L. donovani* Promastigotes

The cytotoxicity of Ag:Se NPs, *P. lanceolata* extract, their combinations, and miltefosine drug was assessed using the MTT assay. Cells infected with *L. donovani* were seeded in 96-well flat-bottom plates with RPMI medium. The infected cells left without any treatment served as the negative control. The positive control included cells treated with miltefosine. Each well of the positive control received 200 µL of medium, followed by 50 µL

of the respective treatment. All treatments were performed in triplicate. The plates were incubated at 26°C for 1, 24, and 48 hrs. At each time point, 10 µL of MTT solution (5 mg/ml in PBS, phosphate-buffered saline) was added to each well and incubated for an additional 4 hrs. After incubation, 100 µL of DMSO was added to dissolve the formazan crystals. Plates were gently shaken for 20 minutes at room temperature to ensure complete solubilization. The absorbance was measured at 620 nm using an ELISA plate reader.

The process was repeated three times, and the cell growth rate was calculated using the equation below [17]. GraphPad Prism v7.14 was used for the statistical analysis of these measurements.

$$\text{Growth Inhibition(GI\%)} = \frac{\text{control cell} - \text{treated cell}}{\text{control}} \times 100\% \quad (\mathbf{1})$$

GraphPad Prism v7.0 is the experimental result to be analyzed, where $*P < 0.5$, $**P < 0.1$, $***P < 0.01$, and $****P < 0.001$.

3. Results and Discussion

3.1. Characterization of NPs: UV-visible Spectrophotometry Study

The results of the UV-Vis analysis showed an absorbance peak at 420 nm for Ag:Se NPs at 125 µg/ml concentration (Fig. 2a), while the 250 µg/mL concentration Ag:Se displayed a broader peak centered around 480 nm (Fig. 2b). These peaks are related to the surface plasmon resonance (SPR) phenomenon, which is common in noble metal nanoparticles like silver. Although the UV-Vis spectrum exhibited some noise, especially at longer wavelengths, the peak positions were reliably identified by smoothing the spectral data with the Savitzky–Golay method and analyzing multiple replicates to confirm the λ_{max} values. The absorption of blue light between 400–450 nm reflects the nanoscale size (40–100 nm) of the synthesized silver nanoparticles [18]. These results are consistent with those of earlier research [19], where Ag@Se core–shell nanoparticles were synthesized with *Ocimum tenuiflorum* extract, showing strong SPR absorbance in the 400–460 nm range, confirming their successful formation and nanoscale dimensions.

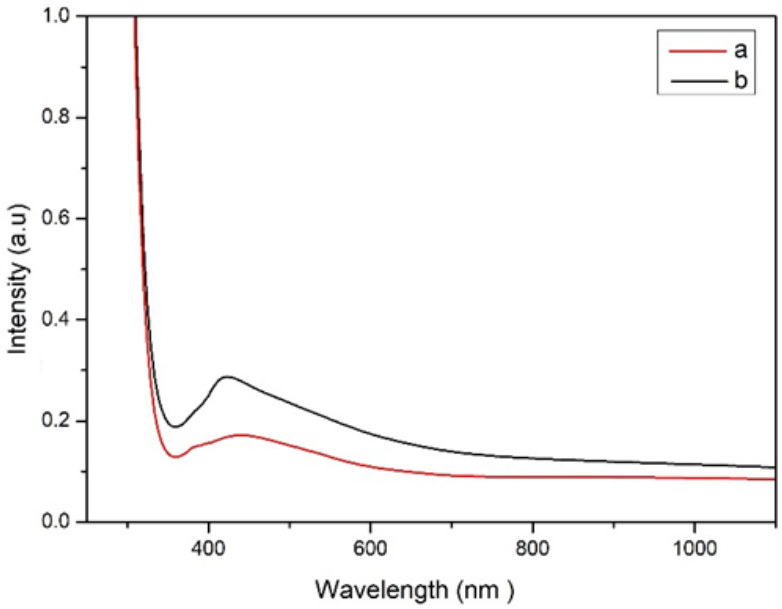

Figure 2: UV-Visible spectra of the prepared Ag:Se nanoparticles of (a)125, (b) 250 µg/ mL concentrations.

3.2. X-Ray Diffraction (XRD) Analysis

Fig. 3 shows the XRD patterns of Ag:Se nanoparticles at two different concentrations of 125 µg/mL (sample a) and 250 µg/mL (sample b). The XRD patterns of the two samples revealed the presence of Ag:Se characteristic peaks, indicating that the synthesis of Ag:Se NPs in the plasma jet was successful [20]. Distinct diffraction peaks appear at 2θ values of 38.15°, 44.25°, 64.5°, and 77.38°, corresponding to the (111), (200), (220), and (311) planes, respectively. These peaks are typical of face-centered cubic (FCC) silver structure, confirming the crystalline nature of silver in both samples. The sample displays sharp and narrow diffraction peaks, reflecting well-defined crystallinity of the silver nanoparticles. Using the Debye–Scherrer equation, Eq. 1, the crystallite size was estimated to be about 72 nm.

$$D = \frac{k\,\lambda}{\beta\cos\theta} \qquad (\mathbf{1})$$

where k is the Scherrer coefficient of 0.9, λ is the X-ray beam wavelength of 0.154 nm, β is the full width at half maximum (FWHM), and θ is the diffraction angle.

The broader background suggests the presence of an amorphous phase or the influence of silver coating on the selenium core, which may obscure selenium's diffraction signals. Sample (b) also showed the characteristic silver peaks but with lower intensity and broader width compared to sample (a). Table 1 presents the crystal size of the prepared Ag:Se NPs at concentrations of 125 and 250 µg/mL. It was noted that the crystallite size increased with the increase in the NPs concentration. However, the decrease in peak sharpness and higher background level might result from increased structural disorder, agglomeration, or heterogeneous distribution of AgNPs on the Se surface. The XRD pattern confirms that all observed peaks correspond to silver and Se phases only, indicating the purity of the synthesized sample and the absence of any external contaminants. The results are consistent with those reported by Al-Shmgani et al. [21], who synthesized silver nanoparticles (Br-AgNPs) via citrate reduction and compared their XRD data with Ag NPs produced using bromelain enzyme. Similarly, in the present study, the diffraction peaks obtained using the Tonkovich approach correspond to the characteristic angles of Ag NPs observed in previous X-ray diffraction analyses.

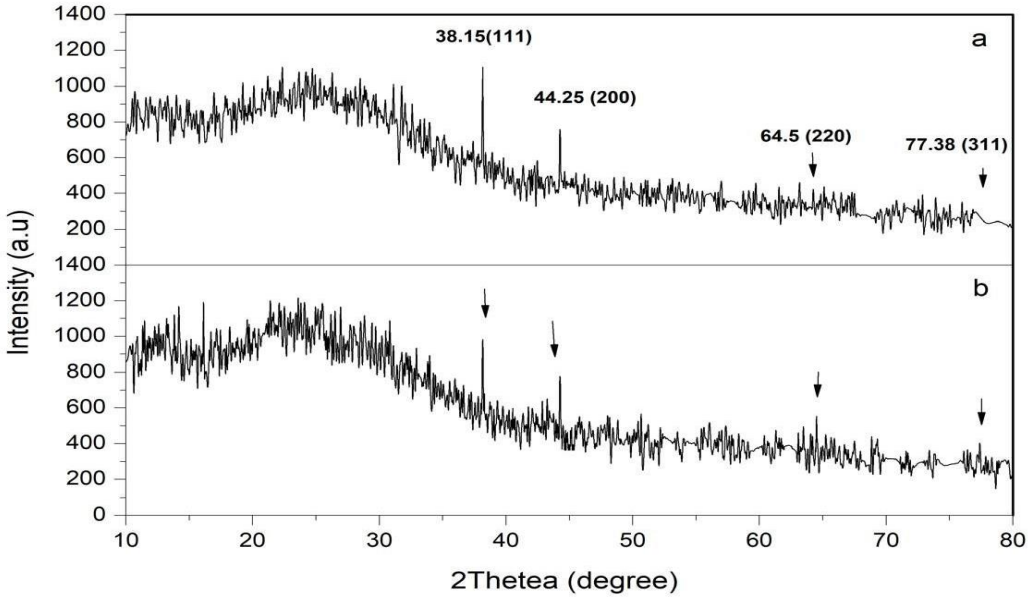

Figure 3: XRD Patterns for Ag:Se NPs of (a) 125, (b) 250 µg/ mL concentrations.

Table 1: Crystal size prepared for Ag:Se NPs of (a) 125, (b) 250 µg/ mL.

Sample	2Ɵ	FWHM	Crystallite size (nm)	Average Crystallite Size (nm)
a	38.1519	0.184	45	72
	44.2744	0.136	63	
	64.5017	0.109	86	
	77.3786	0.1072	94	
b	38.3784	0.12087	69	82
	44.6164	0.1096	78	
	64.4831	0.1056	88	
	77.3786	0.1082	94	

3.4. Scanning Electron Microscopy (SEM) Investigation

SEM images showed the morphological characteristics of the Ag:Se NPs produced using a plasma jet. Ag:Se NPs exhibited spherical shapes with an average particle size of approximately 38–40 nm, as shown in Fig. 4. Regarding particle morphology, the results of the present study are consistent with those reported by Olawale et al. [22], who used *Ocimum tenuiflorum* L. to synthesize silver-core selenium-shell nanoparticles. According to SEM image analysis using ImageJ software, the particle size of Ag:Se NPs was found to be in the range of 38-40 nm, with an average size of approximately 33.1 ± 2.7 nm, based on measurements of more than 100 particles. This result agrees with the study of Ghafoor et al. [23], in which gold nanoparticles synthesized from the extract of pineapple plants, which includes bromelain, had particle sizes ranging from 20 to 60 nm.

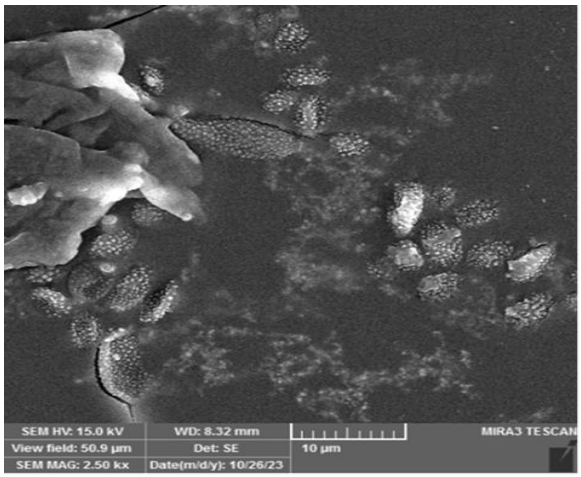

Figure 4: The SEM image of Ag:Se nanoparticles. The scale bar represents 10µm.

3.5. Transmission Electron Microscopy (TEM)

The TEM image in Fig. 5, showing characterization results of the sizes and attributes of the supplied nanoparticles, shows that the Ag:Se NPs in this study had extremely similar morphologies and were both roughly spherical. The NPs formed had near-spherical, pentagonal, and hexagonal shapes as evidenced by TEM. Given that the two employed concentrations of the two sizes of Ag:Se NPs did not significantly differ in their characterization, the results with the greatest concentrations were considered representative. The results of this study, in terms of shapes, are consistent with the results of Olawale et al. [22], where the synthesis of silver-core selenium-shell nanoparticles was done using *Ocimum tenuiflorum* L.

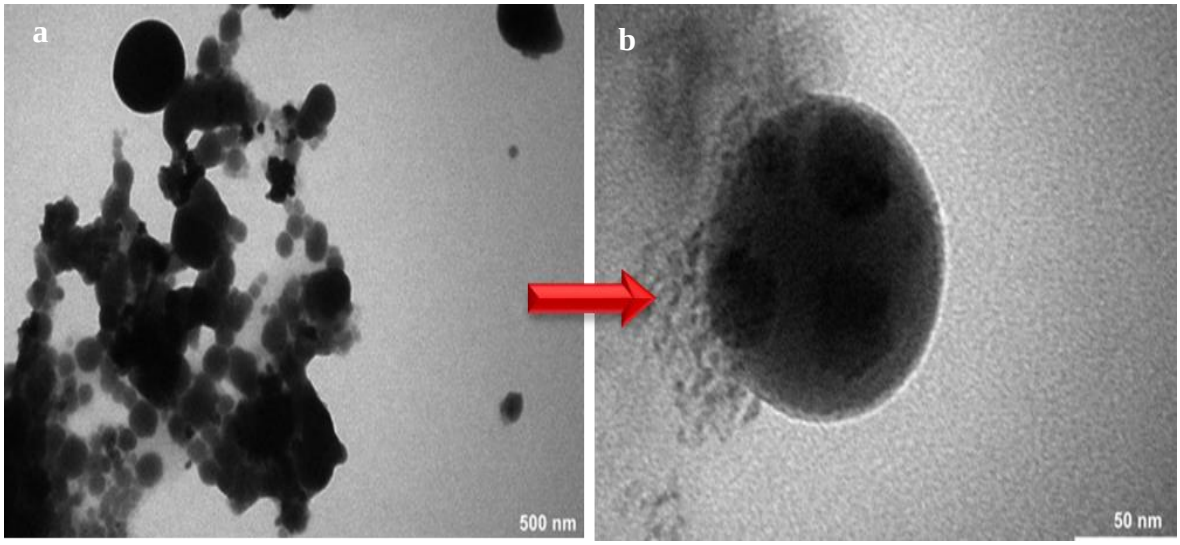

Figure 5: TEM images of Ag:Se NPs; the scale bar represents (a) 500nm, (b) 50nm.

3.6. MTT-Based Cytotoxicity Analysis of Ag:Se NPs Against *L. donovani* in vitro

To assess cell viability and cytotoxicity, the MTT assay was employed, which measures mitochondrial metabolic activity as an indicator of live cells. The reduction of MTT to formazan by viable cells reflects the effectiveness of the treatment. Therefore, a lower absorbance reading corresponds to a higher cytotoxic effect. To determine which treatment evaluation was most effective, the growth inhibition rate of *L. donovani* leishmaniasis when adding Ag:Se at 125 µg/ml and 250 µg/ml concentrations combined with 250 µg/ml *P. lanceolata* was evaluated at 1, 24, and 48 hrs of incubation. After one hour of incubation with 250 µg/mL of Ag:Se NPs at dilutions of 50% and 100%, the percentage of reduction was calculated to be 1.4% and 2.2%, respectively [24], as seen in Figs. 6 and 7. After 24 hrs (Figs. 8 and 9), for the same Ag:Se NPs concentration and the same dilutions, the percentage of reduction was calculated to be 38.4 % and 40.5 %, respectively. The highest anti-leishmanial effect was observed after 48 hrs of incubation (Figs. 10 and 11), which was calculated to be 48.6 % and 59.6 %, respectively.

The findings of this study are consistent with those reported by Jassim et al. [25], who synthesized Cu:Se core–shell nanoparticles using a plasma jet. Their results revealed that the growth inhibition rate of *L. tropica* increased with longer exposure times to the nanoparticles, showing the highest level of parasite destruction after 48 hours, followed by a significant inhibition rate after 24 hrs at a nanoparticle concentration of 100%. Jameii et al. [26] examined the anti-leishmaniasis effect of Se and Ag NPs on *L. major* wound healing. They found that although the diameter of wounds in the nano selenium group did not differ significantly from that of the control group, it did in the case of the nano silver group. It was larger than that of the group that received Glucantime (positive control).

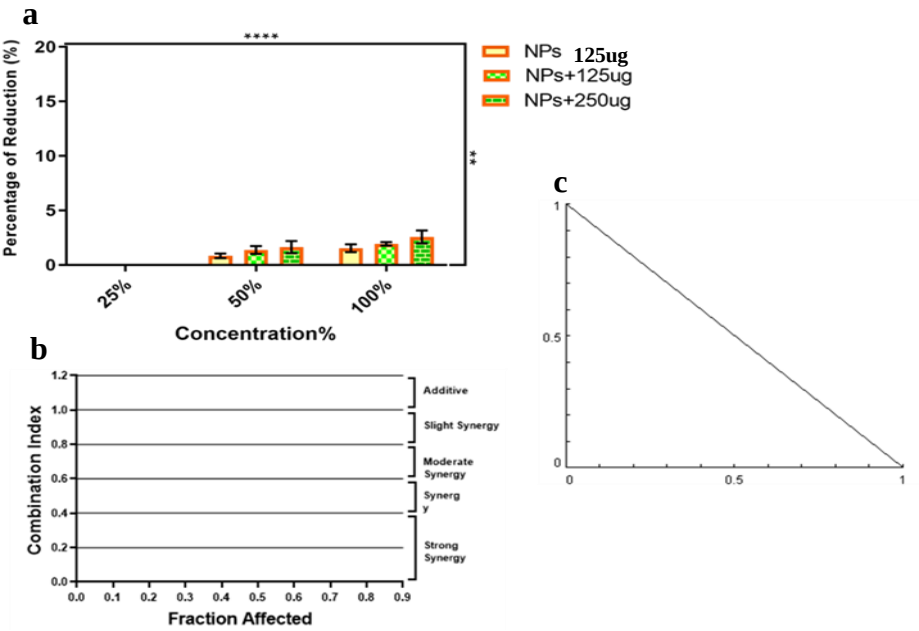

Figure 6: Impact of Ag:Se NPs of 150 µg/ mL concentration on L. donovani after 1-hr incubation (a) Percentage reduction, (b) Combination Index analysis showing the type of Drug Interaction, (c) Isobologram Plot.

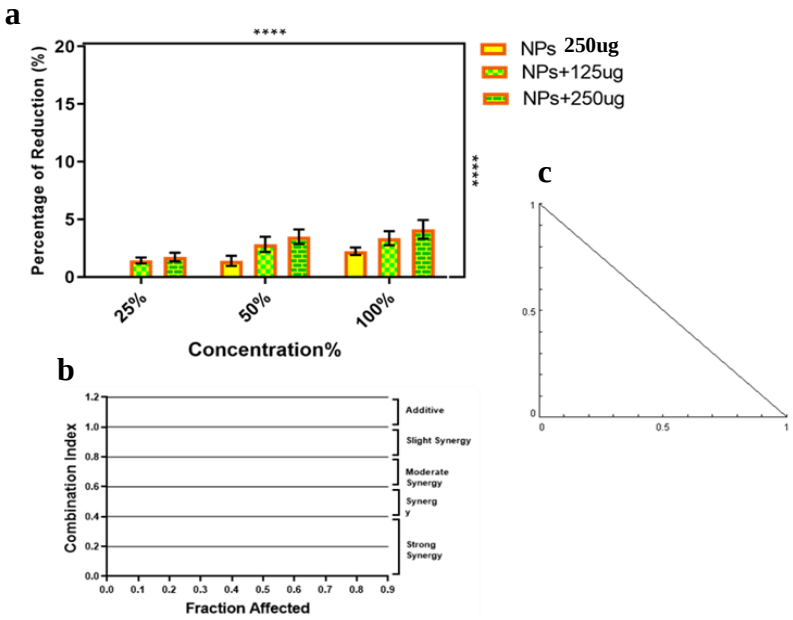

Figure 7: Impact of Ag:Se NPs of 250 µg/ mL concentration on L. donovani after 1-hr incubation (a) Percentage reduction, (b) Combination Index analysis showing the type of Drug Interaction, (c) Isobologram Plot.

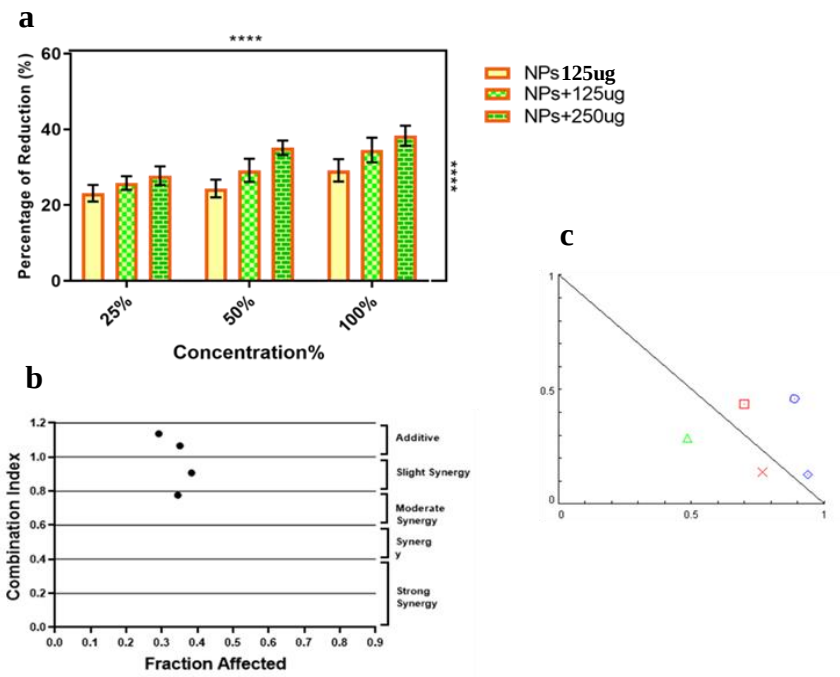

Figure 8: Impact of Ag:Se NPs of 150 µg/ mL concentration on L. donovani after 24-hrs incubation (a) Percentage reduction, (b) Combination Index analysis showing the type of Drug Interaction, (c) Isobologram Plot.

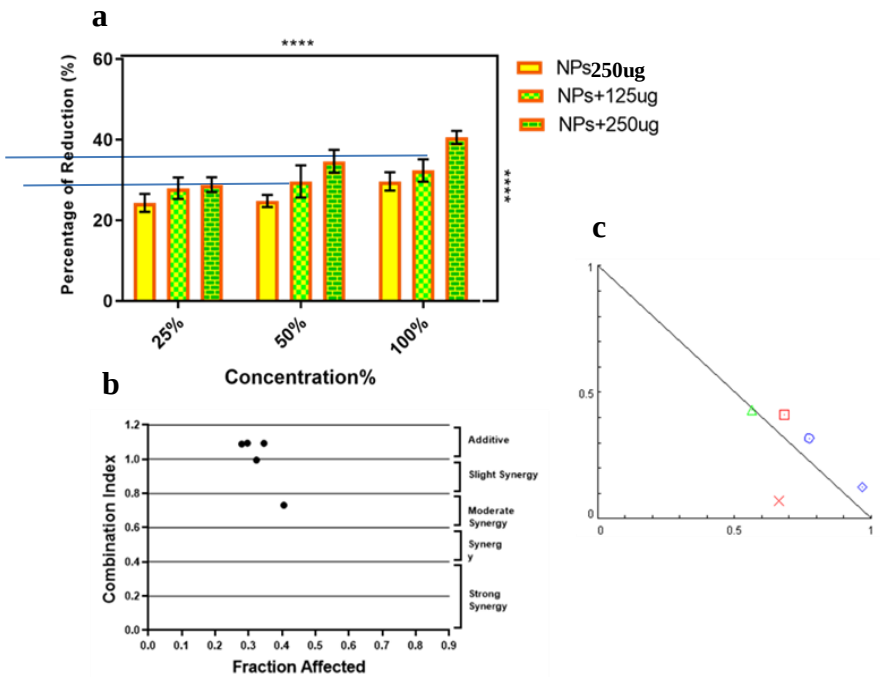

Figure 9: Impact of Ag:Se NPs of 250 µg/ mL concentration on L. donovani after 24-hour incubation (a) Percentage of reduction, (b) Combination Index analysis showing the type of Drug Interaction, (c) Isobologram Plot.

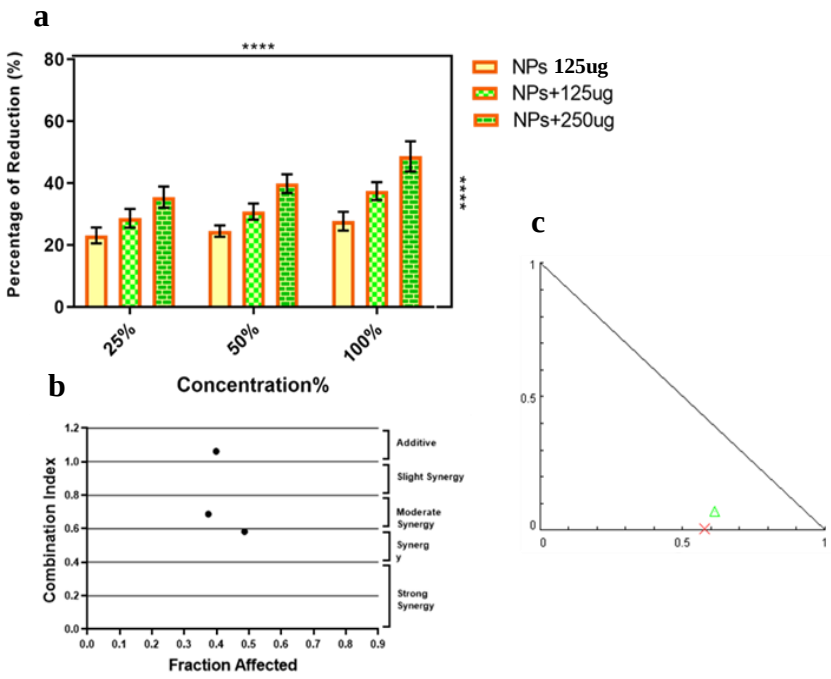

Figure 10: Impact of Ag:Se NPs of 150 µg/ mL concentration on L. donovani after 48-hour incubation (a) Percentage of reduction, (b) Combination Index analysis showing the type of Drug Interaction, (c) Isobologram Plot.

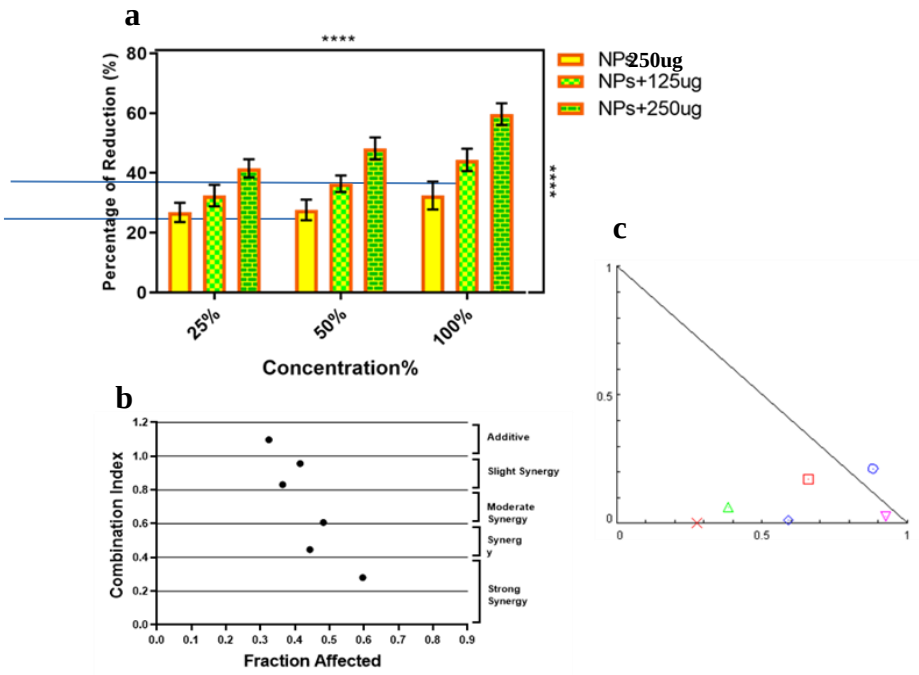

Figure 11: Impact of Ag:Se NPs of 250 µg/ mL comcentration on L. donovani after 48-hour incubation (a) Percentage of reduction, (b) Combination Index analysis showing the type of Drug Interaction, (c) Isobologram Plot.

Fig. 12 shows that the highest anti-leishmanial effect after exposure to the combined *P. lanceolata* extract of 250 µg/mL concentration with the miltefosine drug was 53.1% after 48 hrs of incubation.

The results demonstrated that the inhibition rate of parasite growth increased with longer incubation periods. Furthermore, a synergistic effect was observed in all combination treatments of Ag:Se nanoparticles at concentrations of 125 and 250 µg/mL after 24 and 48 hrs incubation. However, no synergistic effect was detected for the same concentrations of Ag:Se NPs against *L. denevani* after 1 hour of incubation. The present study observed characteristics of programmed cell death, including DNA fragmentation and cell shrinkage, in forms of *L. donovani* (promastigotes) that were treated. Similar to a previous study by Khademvatan et al. [27] involving promastigotes of *L. infantum* exposed to HePC, the investigation similarly demonstrated cell death that exhibited most of the traits associated with metazoan apoptosis.

Furthermore, the drug can induce *L. donovani* promastigotes, *L. amazonensis*, and *L. donovani* intra- and extracellular amastigotes to undergo this kind of deliberate cell death that resembles apoptosis. HePC has demonstrated potential in the fight against malignant cells and *Leishmania* parasites. It has been observed that *Leishmania* promastigotes exposed to reactive oxygen species experience apoptosis-like cell death, which resembles metazoan apoptosis and is characterized by nuclear condensation, DNA fragmentation, and loss of cell volume. Furthermore, the authors suggest that the excessive generation of ROS by nanoparticles leads to direct DNA damage, subsequently causing necrosis followed by apoptosis [28].

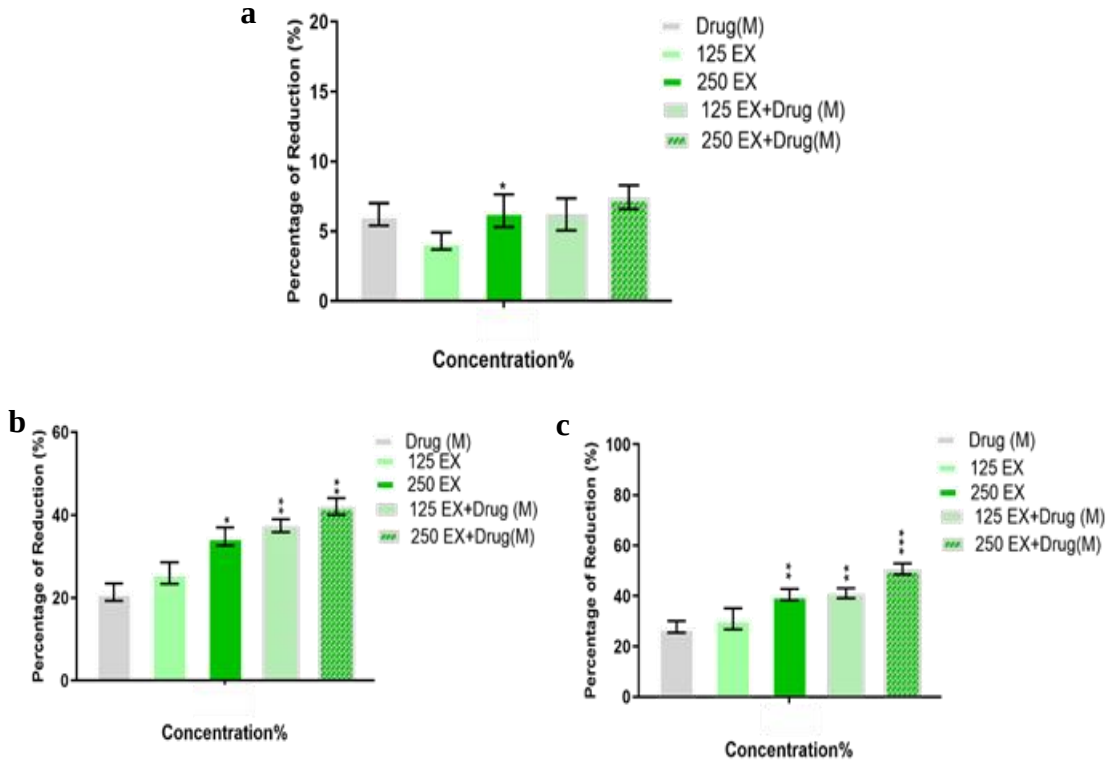

Figure 12: Percentage reduction of L. donovani on exposure to miltefosine, P. Lanceolate extract (EX) at 125 and 250 µg/mL concentrations, and a combination of miltefosine and P. lanceolate extract after (a) 1 hour, (b) 24 hours, (c) 48 hrs' incubation.

4. Conclusions

Diseases caused by parasites, especially *Leishmania donovani*, are well documented. Therefore, using non-side-effect alternative medicines is highly advantageous in combating this parasite. The study results showed that nanoparticles containing *P. lanceolate* extract reduced the parasite population by 59.5 percent after 48 hrs. Most medications, particularly miltefosine, are administered for 21 days, and prolonged infection may lead to parasite death. Compared to other medications that require a longer half-life, the treatment used against promastigotes was effective, achieving a 59.5 percent reduction in parasites after 48 hrs. To eliminate non-healing VL and other chronic intracellular infections, a better approach may be to combine the plant extract or conventional medications with the nano-core: shell formulation, or both.

Conflict of Interest

The authors declare no conflict of interest.

References

1. W. R. Ali, R. S. Al-Sady, and A. J. Al-Saadi, Evaluation of Dot. ELISA test for Diagnosis Visceral Leishmaniasis in infected children, Ibn AL-Haitham Journal for Pure and Applied Science 22, 4 (2017).
2. D. Mabey, E. Agler, J. Amuasi, L. Hernandez, T. Hollingsworth, P. Hotez, P. Lammie, M. Malecela, S. Matendechero, E. Ottesen, and R. Phillips, Towards a comprehensive research and development plan to support the control, elimination and eradication of neglected tropical diseases, *Transactions of The Royal Society of Tropical Medicine and Hygiene*. **115**(2), 196 (2021).
3. D. Peer, J. Karp, S. Hong, O. Farokhzad, R. Margalit, and R. Langer, Nanocarriers as an emerging platform for cancer therapy, *Nat Nanotechnol.* **2**(12), 751 (2020). https://doi.org/10.1038/nnano.2007.387.
4. D. Kulkarni, R. Sherkar, C. Shirsathe, R. Sonwane, N. Varpe, S. Shelke, M. P. More, S. R. Pardeshi, G. Dhaneshwar, V. Junnuthula and S. Dyawanapelly, Biofabrication of nanoparticles: sources, synthesis, and biomedical applications. *Front. Bioeng. Biotechnol.* **11**, 1159193 (2023). https://doi.org/10.3389/fbioe.2023.1159193.
5. T. Lammers, and M. Ferrari, The success of nanomedicine, *Nano Today* **31**(20), 100853(2020). https://doi.org/10.1016/j.nantod.2020.100853.
6. R. Sperling, and W. Park, Surface modification, functionalization and bioconjugation of colloidal inorganic nanoparticles, *Philos Trans A Math Phys Eng Sci.* **368**(1915), 133383 (2010). https://doi.org/10.1098/rsta 2009.0273.
7. N. Kumar, N. Kaushik, N. Nhat, B. Ghimire, A. Pengkit, J. Sornsakdanuphap, S. Lee, and E. Choi, Plasma and Nanomaterials: Fabrication and Biomedical Applications, *Nanomaterials. (***9**(1), 98 (2019). https://doi.org/10.3390/nano9010098.
8. İ. Karakaş, L. B. Sağır and D. N. Hacıoğlu, Biological activities of green synthesis silver nanoparticles by Plantago lanceolata L. leaves. GSC Biological and Pharmaceutical Sciences, **22**(2), 290 (2023). doi.org/10.30574/gscbps.2023.22.2.0079.
9. B. Javed, A. Nadhman, and Z. Mashwani, Phytosynthesis of Ag nanoparticles from Mentha longifolia: their structural evaluation and therapeutic potential against HCT116 colon cancer, Leishmanial and bacterial cells, *Applied Nanoscience* **10**(9), 3503 (2020). https://doi.org/10.1007/s13204-020-01428-5.
10. K. Xiao, B. Zhou, D. Feng, D. S. Yang, S. Lei, D. Wusiman, Z. Jiang, F. Li and M. Liu, Nanotechnology-enabled precision strategies for bladder cancer: from in vitro diagnostics to in vivo therapy. *J Nanobiotechnol* **24**, 780 (2026). https://doi.org/10.1186/s12951-026-04635-4.
11. S. Tamjidi, and A. Ameri, A review of the application of sea material shells as low cost and effective bio-adsorbent for removal of heavy metals from wastewater. *Environ. Sci. Pollut. Res.* **27**, 31105 (2020). https://doi.org/10.1007/s11356-020-09655-7.
12. Y. Huang, Y. Fu, M. Li, D. Jiang, C. J. Kutyreff, J. W. Engle, X. Lan, W. Cai, and T. Chen, Chirality-driven transportation and oxidation prevention by chiral selenium nanoparticles, *Angewandte Chemie*. **59**, 4436 (2020). https://doi.org/10.1002/anie.201910615.
13. C. Ding, C. Yang, T. Cheng, X. Wang, Q. Wang, R. He, S. Sang, K. Zhu, D. Xu, J. Wang, X. Liu, Macrophage-biomimetic porous Se@SiO_2 nanocomposites for dual modal immunotherapy against inflammatory osteolysis. *J. Nanobiotechnol.* **19**, 382 (2021). https://doi.org/10.1186/s12951-021-01128-4.
14. C. Sanmartín, D. Plano, A. Sharma, and J. Palop, Selenium Compounds, Apoptosis and Other Types of Cell Death: An Overview for Cancer Therapy, *Int. J. Mol. Sci.* 13(8), 9649 (2012). doi.org/10.3390/ijms13089649.

15. W. Lin, J. Zhang, J. Xu, and J. Pi, The Advancing of Selenium Nanoparticles Against Infectious Diseases, *Front. Pharmacol.* **12**, 682284 (2021). https://doi.org/10.3389/fphar.2021.682284.
16. H. Abdulalsalam, N. M. Ardalan, and S. H. Ahmed, Evaluation of anti-inflammatory effect by using iron nanoparticles prepared by *Juglans regia* water extract, Current Research in Microbiology and Biotechnology **5**(4), 1151 (2017).
17. B. Adil, K. Aadim, and M. Khalaf, Synthesis and spectroscopic characterization of platinum nanoparticles by plasma jet method, *Int. J. Nanosci.* **20**(3), 2150030 (2021). https://doi.org/10.1142/S0219581X21500307.
18. Kumar, A., Bhatt, S.C., Verma, M., Kumar, V., and Kim, H. Au–Ag core–shell composite nanoparticles as a selective and sensitive plasmonic chemical probe for L-cysteine detection in *Lens culinaris* (lentils), *RSC Adv.* **11**(33), 20390 (2021). https://doi.org/10.1039/d1ra01824h.
19. D. Acharya, B. Mohanta, and P. Pandey, Green synthesis of Silver and Silver-gold core-shell nanoparticles using Pineapple leaf extract (Ananas comosus) and study of their antibacterial properties, *Int. J. Nano Dimens.* **12**(3), 203 (2021).
20. S. Chand, and P. Sharma, Synthesis and characterization of Ag-chalcogenide nanoparticles for possible applications in photovoltaics. *Materials Science-Poland* **36**(3), 375 (2018). https://doi.org/10.2478/msp-2018-0064.
21. H. Al-Shmgani, K. A. Khalil, and H. Mohammed, Synthesis and characterization of proteolytic enzyme loaded on silver nanoparticles, Ibn AL-Haitham Journal for Pure and Applied Sciences. **37**(1), 43 (2024). https://doi.org/10.30526/37.1.3300.
22. F. Olawale, M. Ariatti, and M. Singh, Biogenic synthesis of silver-core selenium-shell nanoparticles using *Ocimum tenuiflorum* l.: response surface methodology-based optimization and biological activity, *Nanomaterials*. **11**(10), 2516 (2021). https://doi.org/10.3390/nano11102516.
23. A. Ghafoor, W. Saod, and N. Mohammed, Green synthesis of gold nanoparticles using pineapple extract and study their analytical characterization and antibacterial activity, *Sys. Rev. Pharm*. **11(**2), 462 (2020). https://doi.org/10.5530/srp.2020.2.70.
24. Z. Jabeer and N. Ardalan, The impact of combination Ag: Se core: shell nanoparticles synthesized by plasma jet with Plantago lanceolata on ref cell line, *J. Physics: Conference Series*, **2857**(1), 012008 (2024). https://doi.org/10.1088/1742-6596/2857/1/012008.
25. D. Jassim, R. Al-Ansari, and B. Adil, Synthesis of Core-Shell Nanoparticles (Cu:Se) by Plasma Jet for Parasitic Leishmaniasis Treatment, *Plasma Medicine*. **13**(4), 21 (2023). https://doi.org/10.1615/PlasmaMed.2023049445.
26. F. Jameii, A. Dalimi, M. Karimi, and F. Ghaffarifar, *Avicenna J. Clin. Med*. **22**(3), 217 (2015**)**.
27. S. Khademvatan, M. J. Gharavi, L. Akhlaghi, A. Samadikuchaksaraei, K. Mousavizadeh, R. Hadighi, and J. Saki, Induction of apoptosis by miltefosine in Iranian strain of *Leishmania infantum* promastigotes. *Iranian J. Parasitol.* **4**, 23 (2009).
28. H. Barabadi, H. Vahidi, K. Damavandi Kamali, M. Rashedi, and M. Saravanan, *J. Cluster Sci.* **31**, 659 (2020). https://doi.org/10.1007/s10876-019-01697-3.

التاثير التآزري لجسيمات النانوية (فضة: سلينيوم) المحضرة بواسطة نفث البلازما الممزوج مع *Leishmania donovani* على اللشمانيا الاحشائية (*Plantago lanceolata*)

زهراء بشير جابر[1] و نخشين ميرزا محمود[1]
[1] قسم الاحياء، كلية العلوم للبنات، جامعة بغداد، بغداد، العراق

الخلاصة
داء الليشمانيات الحشوي عدوى مزمنة تسببها الأوليات. تتطلب الحالات المقاومة للأدوية حلاً عاجلاً لمقاومة الأدوية واستراتيجية علاجية مُحسّنة. تُظهر الجسيمات النانوية المحتوية على مستخلصات نباتية اصطناعية فعالية مضادة لليشمانيا كعوامل علاجية. تهدف هذه الدراسة إلى بحث التأثير التآزري المضاد لليشمانيا لجسيمات نانوية ذات بنية أساسية-غلافية من الفضة والسيلينيوم (Ag:Se) تم تصنيعها باستخدام تقنية نفث البلازما بالاشتراك مع مستخلص أوراق نبات لسان الحمل (Plantago lanceolata) ضد طفيل الليشمانيا الدونوفانية. تم تصنيع جسيمات Ag:Se النانوية وتطبيقها بتركيزين، 125 و250 ميكروغرام/مل، لتقييم فعاليتها المحتملة في المختبر. كان العلاج المرجعي هو الملتيفوسين، وهو دواء مضاد لليشمانيا. استُخدم مستخلص نبات لسان الحمل بتركيزين 125 و250 ميكروغرام/مل لإنتاج جسيمات Ag النانوية كنواة، وأُضيف السيلينيوم كغلاف. تم توصيف جسيمات Ag:Se النانوية المُصنّعة باستخدام مطيافية الأشعة فوق البنفسجية والمرئية، وحيود الأشعة السينية (XRD)، والمجهر الإلكتروني النافذ (TEM)، والمجهر الإلكتروني الماسح (SEM). وقُيّمَ النشاط المضاد لداء الليشمانيات لهذه الجسيمات النانوية. تم تقييمها بتركيزين: 125 و250 ميكروغرام/مل، مع تخفيفات متسلسلة بنسب 25% و50% و100% على مدى فترات حضانة 1 و24 و48 ساعة. بعد 48 ساعة، بلغت نسبة التثبيط لجسيمات Ag:Se النانوية (بتركيزي 125 و250 ميكروغرام/مل) مع المستخلص 48.6% و59.6% على التوالي. وبالتالي، يُستنتج من هذه النتائج أن معدل تثبيط النمو يزداد مع طول فترة حضانة الطفيل. تم تحسين النشاط المضاد لداء الليشمانيات في حالة الأدوية المصنوعة من جسيمات نانوية من الفضة والسيلينيوم (Ag:Se NPs) باستخدام نفث البلازما.

الكلمات المفتاحيه: (فضة: سلينيوم) جسيمات النانويه، اللشمانيا الاحشوية، نفث البلازما، التازر، المجهر الإلكتروني الماسح.